BIOCHEMISTRY
including biophysical chemistry & molecular biology

Contributions of Unique Active Site Residues of Eukaryotic UDP-Galactopyranose Mutases to Substrate Recognition and Active Site Dynamics

Isabel Da Fonseca,[§] Insaf A. Qureshi,[#] Ritcha Mehra-Chaudhary,[†] Karina Kizjakina,[§] John J. Tanner,*[,‡] and Pablo Sobrado*[,§]

[§]Department of Biochemistry, Virginia Tech, Blacksburg, Virginia 24061, United States

[#]Department of Biotechnology and Bioinformatics, School of Life Sciences, University of Hyderabad, Hyderabad, 500046, India

[†]Structural Biology Core and [‡]Departments of Biochemistry and Chemistry, University of Missouri-Columbia, Columbia, Missouri 65211, United States

S *Supporting Information*
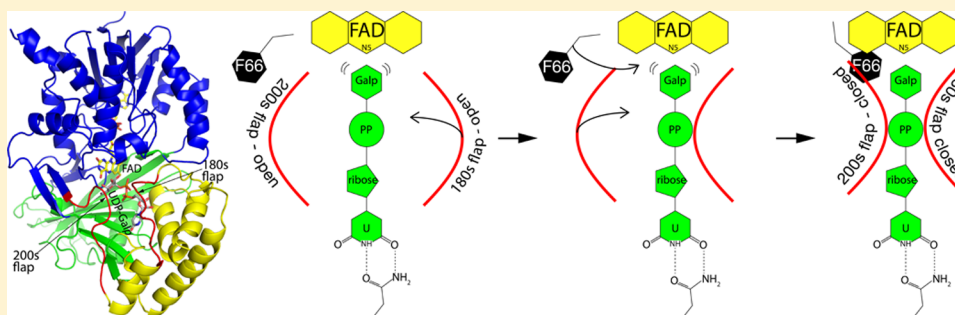
ABSTRACT: UDP-galactopyranose mutase (UGM) catalyzes the interconversion between UDP-galactopyranose and UDP-galactofuranose. Absent in humans, galactofuranose is found in bacterial and fungal cell walls and is a cell surface virulence factor in protozoan parasites. For these reasons, UGMs are targets for drug discovery. Here, we report a mutagenesis and structural study of the UGMs from *Aspergillus fumigatus* and *Trypanosoma cruzi* focused on active site residues that are conserved in eukaryotic UGMs but are absent or different in bacterial UGMs. Kinetic analysis of the variants F66A, Y104A, Q107A, N207A, and Y317A (*A. fumigatus* numbering) show decreases in k_{cat}/K_M values of 200−1000-fold for the mutase reaction. In contrast, none of the mutations significantly affect the kinetics of enzyme activation by NADPH. These results indicate that the targeted residues are important for promoting the transition state conformation for UDP-galactofuranose formation. Crystal structures of the *A. fumigatus* mutant enzymes were determined in the presence and absence of UDP to understand the structural consequences of the mutations. The structures suggest important roles for Asn207 in stabilizing the closed active site, and Tyr317 in positioning of the uridine ring. Phe66 and the corresponding residue in *Mycobacterium tuberculosis* UGM (His68) play a role as the backstop, stabilizing the galactopyranose group for nucleophilic attack. Together, these results provide insight into the essentiality of the targeted residues for realizing maximal catalytic activity and a proposal for how conformational changes that close the active site are temporally related and coupled together.

The cell walls of several fungi and mycobacteria contain galactofuranose (Gal*f*), the five-membered ring of galactose.[1−3] In *Mycobacterium tuberculosis* Gal*f* functions as a linker between the peptidoglycan and the mycolic acid layer.[4] In the human pathogenic fungus *Aspergillus fumigatus*, Gal*f* is an important component in the fungal cell wall assembly, where it is found in galactomannan, glycoproteins, sphingolipids, and lipid-linked glycans.[2] Gal*f* is also a major cell surface virulence factor in several human protozoan parasites.[5−7] Biosynthesis of Gal*f* is initiated by the action of UDP-galactopyranose mutase (UGM), a flavin-dependent enzyme that converts UDP-galactopyranose to UDP-galactofuranose (Scheme 1).[8,9] The reaction catalyzed by UGM does not involve reduction/oxidation of the sugar; however, the UGM activity has been

Scheme 1. Reaction Catalyzed by UGM
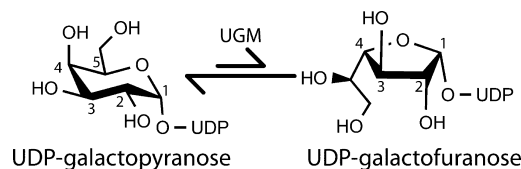
UDP-galactopyranose ⇌ UDP-galactofuranose

shown to have an absolute requirement for the reduced flavin.[10−12] The role of the reduced flavin in the isomerization reaction has been shown to involve the formation of a flavin-galactose adduct. Formation of the flavin-sugar adduct allows ring opening and recyclation to form the furanose. UDP remains bound and acts as a nucleophile producing UDP-Gal*f* and reduced flavin.[13−15] Because the reaction of UGM is essential for Gal*f* biogenesis and the structure and mechanism of this enzyme are unique to microorganisms, UGMs have become major targets for drug design.[9,16,17]

Crystallographic studies established the UGM fold, which consists of three domains (Figure 1A). FAD binds to the Rossmann fold substructure within domain 1. The substrate binds primarily to domains 2 and 3 with the galactopyranose (Gal*p*) moiety near the isoalloxazine and the uridine packed against a helix in domain 2 known as the "uridine wall".[18] The location of the C1 atom of Gal*p* near the N5-FAD atom is consistent with mechanistic studies showing that the N5-FAD atom functions as a nucleophile.[11,14,15,19]
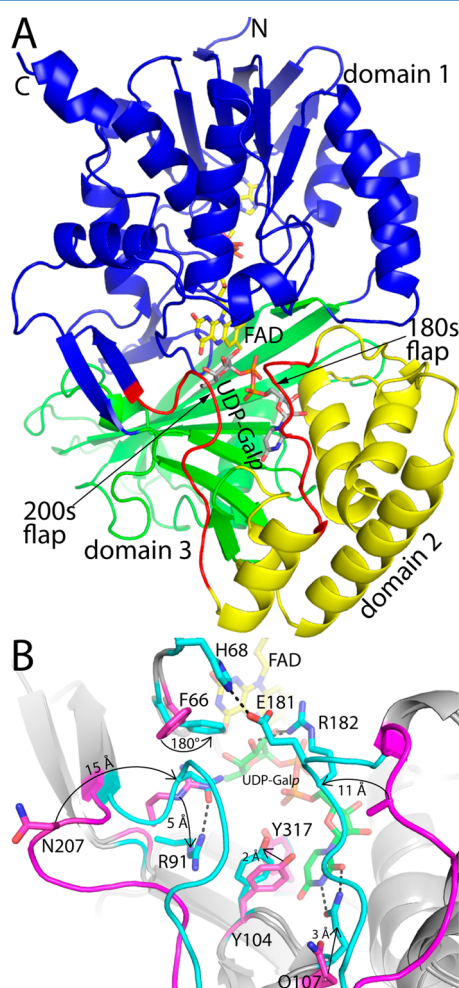
Conformational change linked to substrate binding is an intriguing aspect of UGM, particularly eukaryotic UGMs (eUGMs), which have two mobile active site flaps rather than one as in bacterial UGMs. Structural studies of *Aspergillus fumigatus* UGM (AfUGM) showed that large conformational changes accompany substrate binding.[9,18] The largest of these involve the 180s flap (residues 179−187) and 200s flap (residues 201−209) (Figure 1). In the resting enzyme, the flaps are open and the isoalloxazine is solvent exposed. In complexes with the inhibitor UDP or the UDP-Gal*p* substrate, the flaps are closed and the isoalloxazine and inhibitor/substrate are buried. Closure of the active site requires movements of up to 11 Å for the 180s flap and 15 Å for the 200s flap (Figure 1B). These large conformational changes enable a hydrogen bond between the Gal*p* moiety of the substrate and Arg182, a residue that is conserved in all UGMs. Also, movement of the flaps brings together residues from disparate parts of the sequence to form interactions that presumably stabilize the closed state, such as the His68-Glu181 ion pair and the Arg91-Asn207 hydrogen bond. Other residues exhibit smaller conformational changes associated with substrate binding. Gln107 shifts 3.4 Å to engage the uracil ring, while Tyr104 shifts 2.4 Å to make room for the uracil. Arg91 moves 5 Å to avoid the incoming 200s flap, resulting in a hydrogen bond with Asn207. Finally, the phenyl group of Phe66 rotates 180° to contact the Gal*p* moiety of the substrate, an interaction that has been suggested to help position Gal*p* for nucleophilic attack by the flavin N5.[9,18] Together, these conformational changes assemble the constellation of residues needed to bind the transition state conformation of the substrate, create a protected environment for catalysis, and prevent the severed UDP from migrating out of the active site during catalysis.

Several of the critical residues involved in active site closure are unique to eUGMs. For example, the residues of the 200s flap are found only in eUGMs, reflecting the fact that the bacterial enzymes have only one mobile flap corresponding to the 180s flap of AfUGM. Also, residues near the uridine, such as Gln107, Tyr104, and Tyr317 (AfUGM numbering), are unique to eUGMs, which results in a 5 Å shift in the position of the UMP between the bacterial and eukaryotic enzymes. Arg91 and Phe66 are likewise unique to eUGMs, although bacterial UGMs have a His residue that could play the role of Phe66. These differences in amino acids, along with differences in quaternary structure, are thought to underlie the much larger conformational changes that are associated with substrate binding in eUGMs.

To better understand the origins of substrate recognition and active site dynamics, we have targeted five active site residues of AfUGM and *Trypanosoma cruzi* UGM (TcUGM) that are unique to eUGMs: Phe66, Tyr104, Gln107, Asn207, and Tyr317 (AfUGM numbering). We show that all five residues are important for activity. Furthermore, the crystal structures of the AfUGM variants provide insight into the roles that these residues play in substrate recognition and facilitating the protein conformational changes that are associated with formation of the E-S complex.

Figure 1. Conformational changes and the structural context of residues targeted for mutagenesis. (A) Protomer structure of AfUGM complexed with UDP-Gal*p* (PDB code 3UTH). Structural domains 1, 2, and 3 are colored blue, yellow, and green, respectively. The mobile active site flaps are colored red. FAD and UDP-Gal*p* are colored yellow and gray, respectively. (B) Comparison of the open active site of ligand-free AfUGM (magenta) and closed active site of AfUGM complexed with UDP-Gal*p* (cyan). The arrows indicate the conformational changes associated with the binding of UDP-Gal*p* (or UDP) to AfUGM. FAD and UDP-Gal*p* are colored yellow and green, respectively.

■ EXPERIMENTAL PROCEDURES

Materials. UDP and UDP-Gal*p* were purchased from Sigma. UDP-Gal*f* was synthesized following the chemo-enzymatic procedure developed by the Lowary group.[20] Pfu

Ultra Hotstart High-Fidelity DNA polymerase was obtained from Agilent Technologies. DpnI was from Fisher. *Escherichia coli* TOP-10 chemical competent cells were obtained from Invitrogen. *E. coli* BL21 (DE3) chemical competent cells were from Promega (Madison, WI). The plasmid miniprep kit was from Qiagen. Primers were from Integrated DNA Technology (IDT). All other buffers and chemicals were purchased from Fisher Scientific.

Site-Directed Mutagenesis. Primers were designed to create the following point mutations of conserved unique active site eUGM residues: AfUGMF66A, AfUGMY104A, AfUGM-Q107A, AfUGMN207A, AfUGMY317A, TcUGMY100A, TcUGMQ103A, TcUGMN201A, and TcUGMY317F. In prokaryotic UGMs the residue equivalent to F66 in AfUGM is a His residue (Supporting Information Figure S1).[9] In the *Mycobacterium tuberculosis* UGM (MtUGM) this residue corresponds to His68. In order to determine the role of this residue the MtUGMH68A mutant was created. Site-directed mutagenesis was performed following the manufacturer's instructions (QuikChange Site-Directed Mutagenesis Kit) using as template the double mutant AfUGMK344A/K345A gene cloned into pVP55A, while the TcUGM and MtUGM genes were cloned into pVP56K.[12,15] The mutations were confirmed by DNA sequencing.

Protein Expression and Purification. Expression and purification of wild-type AfUGM and all mutants were done under conditions previously reported.[12,15] Similarly, TcUGM and MtUGM variants were expressed and purified following published protocols.[12,15] In general, from ~60 g of cell paste (6 L of autoinduction media[21]), ~15 mg of purified protein was isolated. Protein quantitation was performed by measuring the flavin absorbance at 452 nm and using an extinction coefficient of 10.5 mM^{-1} cm^{-1} for AfUGM and 10.8 mM^{-1} cm^{-1} for TcUGM and MtUGM.[12,15] No significant changes in the flavin spectra were observed in any of the mutant enzymes. The AfUGMK344A/K345A isoform was used, as this enzyme can form good quality diffracting crystals.

Mutase Activity Assay. The enzymatic activity of recombinant UGMs was tested by monitoring the formation of UDP-Gal*p* from UDP-Gal*f* by HPLC. The assay was performed in 0.1 mL of 25 mM HEPES, 125 mM NaCl, 20 mM dithionite, at pH 7.5, at various concentrations of UDP-Gal*f*. The reaction was initiated by addition of enzyme at 50 nM for wild-type AfUGM, 1−3 μM for AfUGM mutants, 100 nM for wild-type TcUGM, 0.5−3 μM for TcUGM mutants, 15 nM for wild-type MtUGM, and 500 nM for the MtUGMH68A. The reaction was incubated at 37 °C until ~30% conversion of UDP-Gal*f* to UDP-Gal*p* was achieved. The reaction was terminated by heat denaturation at 95 °C for 5 min, in a DNA engine thermocycler (BioRad, Hercules, CA). After centrifugation, the resulting mixture was injected onto a PA-100 (Dionex) HPLC column. The sample was eluted isocratically with 75 mM KH_2PO_4, pH 4.5, at 0.80 mL/min. Absorbance at 262 nm was monitored to identify fractions containing substrate and product. Under these conditions, UDP-Gal*p* eluted at 27.35 min and UDP-Gal*f* at 34.19 min. The extent of conversion was determined by comparing the integration of the substrate and product peaks. The initial velocity data was fit to the Michaelis−Menten equation to obtain the k_{cat} and K_M values.

Flavin Reduction Assay. Wild-type and mutant forms of AfUGM were analyzed using stopped-flow kinetic experiments as previously described.[22] Briefly, the enzyme and NADPH

were mixed under anaerobic conditions at 15 °C (in 50 mM sodium phosphate, pH 7.0), and the reaction was monitored by measuring the decrease in flavin absorbance at 452 nm. The absorbance changes were fit to eq 1, which describes a single exponential process where A is the absorbance at 452 nm, k_{obs} represents the first-order rate constant associated with the absorbance changes, B is the amplitude of the change, and C is the final absorbance. Kinetic parameters for the reduction of the enzyme as a function of NADPH were obtained by fitting the k_{obs} values to eq 2, where k_{red} is the rate constant for flavin reduction, and K_D is the dissociation constant for NADPH.

$$A = B \ e^{-(k_{obs} \times t)} + C \tag{1}$$

$$k_{obs} = \frac{k_{red}[NADPH]}{K_D + [NADPH]} \tag{2}$$

Crystallization of AfUGM Variants and Crystal Soaking. To aid crystallization, the active site mutations of AfUGM were made on the background of the K344A/K345A double surface mutant of AfUGM. As described previously, K344A/K345A is amenable to high resolution X-ray crystallography, whereas crystals of the wild-type enzyme exhibit translational pseudosymmetry and weak diffraction.[18] Residues 344 and 345 are on the surface of the enzyme, far from the active site and oligomerization interfaces; the kinetic constants of K344A/K345A are virtually identical to those of the native enzyme.[18]

Hexagonal crystals of oxidized AfUGM mutant enzymes AfUGMF66A, AfUGMY104A, AfUGMQ107A, AfUGM-N207A, and AfUGMY317A were grown as described previously.[18] Briefly, the crystals were grown in sitting drops at room temperature with a reservoir solution containing 1.2−1.4 M ammonium sulfate and 0.1 M sodium acetate at pH 4.5. Equal volumes of protein solution and reservoir solution were mixed, and large yellow hexagonal crystals were obtained. The protein stock solution consisted of 5−9 mg/mL enzyme in a buffer of 125 mM NaCl and 25 mM HEPES at pH 7.5. Tris(3-hydroxypropyl)phosphine was added to the protein solution to a final concentration of 1 mM just prior to setting up crystallization experiments. The space group is $P6_522$ with unit cell lengths of a = 217 Å and c = 321 Å. The asymmetric unit contains one tetramer and 75% solvent.

Crystals of reduced, ligand-free AfUGM mutant enzymes were obtained by exchanging the mother liquor of the respective oxidized crystal with a reducing cryobuffer containing 1.6 M ammonium sulfate, 0.2 M sodium acetate pH 4.5, 25% ethylene glycol or glycerol, and 80 mM dithionite. We note that AfUGM is fully reduced in solution by 80 mM dithionite.[23] The yellow color of the crystals was bleached upon soaking, consistent with reduction. When the color transformation was complete (2−3 min), the crystals were plunged into liquid nitrogen to trap the reduced state.

Crystals of reduced AfUGMF66A, AfUGMN207A, and AfUGMY317A complexed with UDP were obtained by exchanging the mother liquor with the reducing cryobuffer supplemented with 200 mM UDP. We note that the conformational changes attendant to UDP binding are identical to those associated with UDP-Gal*p* binding, thus, UDP is a good surrogate ligand for studying substrate recognition by AfUGM.[18] Furthermore, UDP is more soluble and less expensive than UDP-Gal*p*, so it is preferable for crystal soaking trials that require high ligand concentrations (e.g., 200 mM) to achieve high binding occupancy. The soaking times were 12

min for AfUGMF66A, 30 min for AfUGMN207A, and 30 min for AfUGMY317A. Analogous soaking experiments performed with crystals of AfUGMY104A and AfUGMQ107A did not yield convincing electron density features for bound UDP and, thus, only the ligand-free reduced enzyme structures are reported for these variants. A crystal of reduced AfUGMF66A was also soaked in 100 mM UDP-Gal$p$ for 75 min.

X-ray Diffraction Data Collection and Refinement. Diffraction data were collected on beamline 4.2.2 of the Advanced Light Source using a Taurus-1 CMOS detector in shutterless mode and beamlines 24-ID-E and 19-ID of the Advanced Photon Source using ADSC Quantum 315 detectors in conventional shuttered mode. The data were integrated using XDS[24] and scaled with SCALA.[25,26] Amplitudes were inferred from intensities with CTRUNCATE.[26] Data processing statistics are listed in Tables 3 and 4.

Crystallographic refinement calculations for the ligand free structures were initiated from protein coordinates derived from either the 2.25 Å resolution structure of reduced AfUGM (Protein Data Bank (PDB) code 3UTF) or the 2.25 Å resolution structure of reduced AfUGM complexed with UDP (PDB code 3UTG). These calculations were performed with PHENIX.[27] The B-factor model consisted of an isotropic B-factor for each atom and TLS refinement using one TLS group per protein chain. COOT was used for model building.[28] The test set of reflections used for cross validation corresponded to the one used in previous refinements of this crystal form of AfUGM.[18,22] The structures were validated using MolProbity[29] and the PDB validation server. Ramachandran plots were generated with RAMPAGE[30] through the PDB validation server. Refinement statistics are listed in Tables 3 and 4. Coordinates and structure factor amplitudes have been deposited in the PDB under the accession numbers listed in Tables 3 and 4.

■ RESULTS

Flavin Activation. UGMs are active only in the reduced form.[10−12,15] In eUGMs reduction occurs by reaction with NADPH.[15,22,31] In order to test if the residues targeted in this study play a role in the activation process, the rate of flavin reduction and the binding affinity for NADPH were determined in the stopped flow spectrophotometer under anaerobic conditions. No significant changes were determined in the k_{red} values for the AfUGM variants (Table 1), suggesting that these residues are not involved in transition state stabilization for the hydride transfer step. Only minor changes in the K_D values were measured, which resulted in a less than 4-fold change in the k_{red}/K_D (Table 1). These results are

Table 1. Kinetic Parameters for the Reduction of AfUGM Mutant Enzymes by NADPH

	k_{red} (s^{-1})	K_d (μM)	k_{red}/K_d (M^{-1} s^{-1})	relative change
AfUGM	3.00 ± 0.08	25 ± 2	120000 ± 10000	1
F66A	2.40 ± 0.01	27 ± 1	90000 ± 3000	0.74
Q107A	2.50 ± 0.03	21 ± 2	112000 ± 10000	0.99
Y104A^a	2.20 ± 0.04	54 ± 4	41000 ± 3000	0.34
N207A	3.00 ± 0.03	43 ± 2	70000 ± 3000	0.58
Y317A^a	3.40 ± 0.10	100 ± 10	30000 ± 3000	0.28

^{a}Data from Dhatwalia et al.[22]

consistent with the reductive/activation process being largely unaffected by the mutations.

Effect on Mutase Activity. The equilibrium of the UGM reaction favors the formation of the pyranose sugar 17:1.[32] Thus, to allow significant product accumulation for accurate measurement, the activity was monitored in the reverse direction, UDP-Gal$p$ from UDP-Gal$f$. The results are shown in Table 2. All the mutants were active; however, major changes in the k_{cat} values were measured (15- to 500-fold decrease). In addition, the mutants AfUGMF66A and AfUGMQ107A displayed significant increases in K_M. AfUGMQ107A has a 20-fold higher K_M than the wild-type enzyme. AfUGMF66A is notable in that it could not be saturated with UDP-Gal$f$ in the kinetic assays, and so only the ratio of k_{cat} to K_M could be determined. Almost identical effects are observed in the MtUGMH68A, where saturation could not be obtained due to an apparent high K_M value (Table 2). The TcUGM variants displayed similar catalytic deficiencies as the corresponding AfUGM mutants, indicating a conserved role of these residues in the eUGM family of enzymes (Table 2). Inspection of the k_{cat}/K_M values of all the mutant enzymes studied here shows a decrease of 100−1000, suggesting that these residues play important roles in catalysis.

Crystal Structures of Ligand-Free AfUGM Variants. The crystal structures of reduced AfUGM variants AfUGM-F66A, AfUGMY104A, AfUGMQ107A, AfUGMN207A, and AfUGMY317A were determined to high resolution limits of 2.05−2.30 Å (Table 3). All four structures exhibit the three-dimensional signatures of the reduced enzyme,[22] such as butterfly bending of the isoalloxazine, donation of a hydrogen bond from the N5-FADH$_2$ atom to the carbonyl of Gly62, and hydrogen bonding between the imidazole of His63 and the flavin ribityl O2′. None of the mutations have a noticeable effect on the structure of the ligand-free, reduced enzyme. For example, the pairwise root-mean-square deviations (RMSDs) between the tetramers of the mutant and wild-type enzymes span the range 0.2−0.5 Å for Cα atoms. For reference, the RMSDs between the individual protomers of wild-type enzyme structure are 0.2−0.3 Å. Within 10 Å of the mutation, the RMSD for all atoms is 0.1−0.7 Å (calculated after superposition of the tetramer). Thus, the mutations do not induce large global or local conformational changes. These results suggest that the catalytic defects of the mutant enzymes are not due to perturbation of the resting enzyme structure.

Crystal Structures in Complex with UDP. The structures of reduced AfUGMF66A, AfUGM207A, and of AfUGMY317A with UDP were determined at 2.05−2.30 Å resolution (Table 4). *In crystallo* flavin reduction was obtained by soaking crystals of the oxidized enzyme simultaneously in UDP and dithionite. We note that the conformational changes attendant to UDP binding are identical to those associated with UDP-Gal$p$ binding; thus, UDP is a good surrogate ligand for studying substrate recognition by AfUGM.[18] Detailed analysis of each structure is provided below.

Crystal Structure of AfUGMF66A-UDP. Electron density maps clearly indicated that UDP was bound in the active sites of two protomers (chains A and B) of the tetramer in the asymmetric unit (Figure 2A). Half-site binding is also observed in structures of the wild-type enzyme complexed with UDP or UDP-Gal$p$.[18] Weak density for the ribose and pyrophosphate is also evident in a third chain (chain C) but UDP was not modeled in this site.

Table 2. Steady-State Kinetic Parameters for UGM Variants[a]

mutants	k_{cat}, s^{-1}	K_M (μM)	k_{cat}/K_M, M^{-1} s^{-1}	relative change[b]
AfUGM				
Wild-type	72 ± 4	110 ± 15	650000 ± 90000	1
F66A	ND[c]	ND	3500 ± 120	0.005
Y104A	0.17 ± 0.015	57 ± 17.5	3000 ± 700	0.005
Q107A	4.7 ± 0.80	2153 ± 570	2000 ± 200	0.003
N207A	0.13 ± 0.02	166 ± 73	800 ± 200	0.001
Y317A	0.28 ± 0.04	380 ± 129	700 ± 200	0.001
TcUGM				
Wild-type	13.4 ± 0.3	140 ± 10	90000 ± 6000	1
Y100A	0.03 ± 0.002	32 ± 12	800 ± 300	0.008
Q103A	0.14 ± 0.002	478 ± 172	300 ± 60	0.003
N201A	ND[c]	ND	60 ± 10	0.0006
Y317F	0.30 ± 0.01	334 ± 38	860 ± 60	0.009
MtUGM				
Wild-type	71 ± 3	78 ± 16	910000 ± 150000	1
H68A	ND	ND	8000 ± 200	0.008

[a]All the kinetic parameters are with UDP-Gal$f$ as substrate in the presence of 20 mM dithionite. [b]Calculated by dividing the k_{cat}/K_M value for the mutant enzyme by the value for the wild-type enzyme. [c]Not determined due to the high K_M value.

Table 3. X-ray Diffraction Data Collection and Refinement for AfUGM Ligand-Free Structures[a]

	F66A	Y104A	Q107A	N207A	Y317A
beamline	APS 19-ID-D	APS 24-ID-E	APS 24-ID-E	APS 24-ID-E	APS 24-ID-E
space group	$P6_5 22$	$P6_5 22$	$P6_5 22$	$P6_5 22$	$P6_5 22$
unit cell parameters (Å)	a = 217.1, c = 320.3	a = 218.4, c = 322.2	a = 216.2, c = 318.8	a = 218.2, c = 321.9	a = 216.6, c = 317.3
wavelength (Å)	0.97916	0.97918	0.97918	0.97918	0.97918
resolution (Å)	48.4−2.05 (2.09−2.05)	163.1−2.30 (2.34−2.30)	159.4−2.20 (2.24−2.20)	122.5−2.30 (2.34−2.30)	187.5−2.30 (2.34−2.30)
observations	1970641	2130460	1289710	954588	2033601
unique reflections	273170	198787	219305	197338	191862
$R_{merge}(I)$	0.145 (1.081)	0.204 (0.759)	0.138 (0.864)	0.167 (1.167)	0.286 (1.245)
$R_{meas}(I)$	0.156 (1.175)	0.215 (0.796)	0.151 (0.952)	0.189 (1.312)	0.303 (1.312)
$R_{pim}(I)$	0.058 (0.455)	0.065 (0.236)	0.060 (0.388)	0.083 (0.572)	0.095 (0.409)
Mean I/σ	9.0 (2.1)	10.0 (3.1)	10.0 (2.1)	7.6 (1.4)	7.0 (2.0)
Mean $CC_{1/2}$	0.994 (0.640)	0.991 (0.819)	0.995 (0.715)	0.979 (0.563)	0.975 (0.622)
completeness (%)	99.5 (99.9)	99.9 (99.9)	99.7 (100.0)	99.5 (99.9)	99.7 (100.0)
multiplicity	7.2 (6.5)	10.7 (11.2)	5.9 (5.8)	4.8 (4.9)	10.6 (10.8)
no. of protein residues	2020	2020	2020	2020	2020
no. of atoms	16989	16803	16783	16738	16627
no. of FADH$_2$ atoms	212	212	212	212	212
no. of water molecules	1014	861	828	768	716
R_{cryst}	0.1824 (0.2958)	0.1818 (0.2447)	0.1736 (0.2465)	0.1885 (0.2760)	0.2037 (0.3017)
R_{free}[b]	0.2139 (0.3244)	0.2197 (0.3317)	0.2070 (0.3004)	0.2217 (0.3213)	0.2441 (0.3532)
rmsd bond lengths (Å)	0.007	0.007	0.007	0.008	0.008
rmsd bond angles (deg)	1.031	1.023	1.061	1.061	1.087
Ramachandran plot[c]					
favored (%)	98.46	98.11	98.21	98.66	97.81
outliers (residues)	0	0	0	0	0
MolProbity score (%-tile)	100	100	100	100	100
Average B (Å^2)					
protein	33.8	28.9	32.6	37.2	36.2
FADH$_2$	28.6	23.9	27.8	32.7	32.3
water	36.1	31.3	34.1	37.7	35.9
coordinate error (Å)[d]	0.23	0.27	0.23	0.29	0.32
PDB code	4U8I	4U8J	4U8K	4U8L	4U8M

[a]Values for the outer resolution shell of data are given in parentheses. [b]A common 5% test set was used for all refinements. [c]The Ramachandran plots were generated with RAMPAGE[30] via the PDB validation server. [d]Maximum likelihood-based coordinate error estimate reported by PHENIX.

UDP bound to AfUGMF66A adopts the same conformation and interactions that are observed in the wild-type complex (Figure 2). In both structures, the uracil is sandwiched between the aromatic rings of Tyr104 and Phe158 and forms hydrogen bonds with Gln107. The ribose group hydrogen bonds to Asn163 and Trp167, while the pyrophosphate is stabilized by

Table 4. X-ray Diffraction Data Collection and Refinement for AfUGM Complex Structures[a]

|	F66A-UDP	F66A-UDP-Gal*p*	N207A-UDP	Y317A-UDP
beamline	APS 19-ID-D	APS 24-ID-E	ALS 4.2.2	ALS 4.2.2
space group	$P6_522$	$P6_522$	$P6_522$	$P6_522$
unit cell parameters (Å)	$a = 218.5, c = 321.1$	$a = 217.9, c = 321.1$	$a = 218.4, c = 321.7$	$a = 217.2, c = 320.9$
wavelength (Å)	0.97916	0.97918	1.000	1.000
resolution (Å)	48.7−2.30 (2.34−2.30)	162.7−2.20 (2.24−2.20)	63.0−2.30 (2.34−2.30)	61.0−2.05 (2.09−2.05)
observations	3594406	2997337	4448690	2047696
unique reflections	198868	224393	198780	275353
$R_{merge}(I)$	0.177 (1.411)	0.174 (1.403)	0.145 (1.275)	0.113 (1.045)
$R_{meas}(I)$	0.182 (1.455)	0.181 (1.459)	0.148 (1.305)	0.122 (1.124)
$R_{pim}(I)$	0.043 (0.347)	0.048 (0.392)	0.031 (0.277)	0.043 (0.403)
mean I/σ	14.3 (2.3)	13.1 (2.0)	23.6 (2.9)	14.4 (2.4)
mean $CC_{1/2}$	0.998 (0.710)	0.997 (0.565)	0.999 (0.847)	0.998 (0.775)
completeness (%)	99.8 (96.1)	99.7 (100.0)	100.0 (100.0)	99.9 (99.9)
multiplicity	18.1 (16.8)	13.4 (13.8)	22.4 (22.0)	7.4 (7.3)
no. of protein residues	2020	2020	2019	2020
no. of atoms	16357	16334	16652	17305
no. of $FADH_2$ atoms	212	212	212	212
no. of UDP molecules				
active site	2	2	2	4
exosite	2	0	4	3
no. of water molecules	412	536	640	1218
R_{cryst}	0.1756 (0.2830)	0.1878 (0.2894)	0.1728 (0.2284)	0.1676 (0.2476)
R_{free}[b]	0.2091 (0.3135)	0.2208 (0.3373)	0.2028 (0.3009)	0.1932 (0.2893)
rmsd bond lengths (Å)	0.008	0.007	0.007	0.007
rmsd bond angles (deg)	1.069	1.070	1.049	1.030
Ramachandran plot[c]				
favored (%)	98.36	97.91	98.21	98.46
outliers (residues)	0	1	3	0
MolProbity score (%-tile)	100	100	100	100
Average B (Å²)				
Protein	44.9	40.4	43.1	29.9
$FADH_2$	38.0	33.7	35.2	25.2
Active site UDP	35.5	47.7	56.5	61.8
Exosite UDP	73.9	-	69.3	50.7
Water	40.4	37.4	42.9	35.1
UDP occupancies				
active site UDP	0.94, 1.0	0.85	0.85, 0.91	0.79−0.83
exosite UDP	0.76, 0.84	-	0.78−0.87	0.79−0.86
Coordinate error (Å)[d]	0.24	0.26	0.23	0.18
PDB code	4U8N	4WX1	4U8O	4U8P

[a]Values for the outer resolution shell of data are given in parentheses. [b]A common 5% test set was used for all refinements. [c]The Ramachandran plots were generated with RAMPAGE[30] via the PDB validation server. [d]Maximum likelihood-based coordinate error estimate reported by PHENIX.

electrostatic interactions with Arg327 and three Tyr side chains (317, 419, 453). Both active site flaps are closed in AfUGMF66A-UDP, as in the wild-type enzyme complexes with UDP or UDP-Gal*p*. The C*α* RMSD between AfUGMF66A-UDP and the wild-type UDP complex is only 0.1 Å for the 180s flap and 0.2 Å for the 200s flap, indicating nearly identical flap conformations in the two structures. In summary, AfUGMF66A-UDP mimics the Michaelis E-S complex except for the obvious absences of the Phe66 side chain and Gal*p* group. The fact that AfUGMF66A has 200-fold lower k_{cat}/K_M (Table 1) suggests that Phe66 plays an important role in catalysis that is unrelated to flap closure and establishing the correct conformation of the UDP part of the substrate.

An additional structure was determined from a reduced AfUGMF66A crystal soaked in 100 mM UDP-Gal*p* (Table 4). Although electron density for the UDP moiety is strong and indicates nearly full occupancy, density in the region expected

for Gal*p* is diffuse and disconnected from the UDP (Supporting Information Figure S2). Thus, it was not possible to build the Gal*p* moiety with confidence. It is possible that the lack of Phe66 in this mutant induces conformational disorder in Gal*p*, implying that Phe66 plays a role in stabilizing Gal*p* for nucleophilic attack. However, we caution that conformational disorder of the Gal*p* moiety has been observed even in wild-type UGM-UDP-Gal*p* structures, including AfUGM (PDB codes 3UKH and 3UKF (especially chain E)[33] and *Klebsiella pneumoniae* UGM (PDB code 3INT, chain A).[14] Nevertheless, this structure appears to be consistent with Phe66 playing the role of the Gal*p* backstop.

Crystal Structure of AfUGMN207A-UDP. In this complex, the electron density maps showed that UDP is bound in the active sites of protomers A and B (Figure 3A). Occupancy refinement indicated occupancies of 0.85 in chain A and 0.91 in chain B (Table 4). We focus on protomer B below.
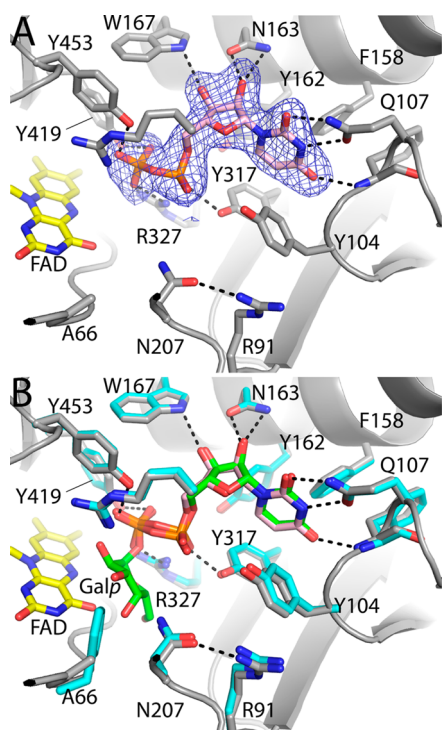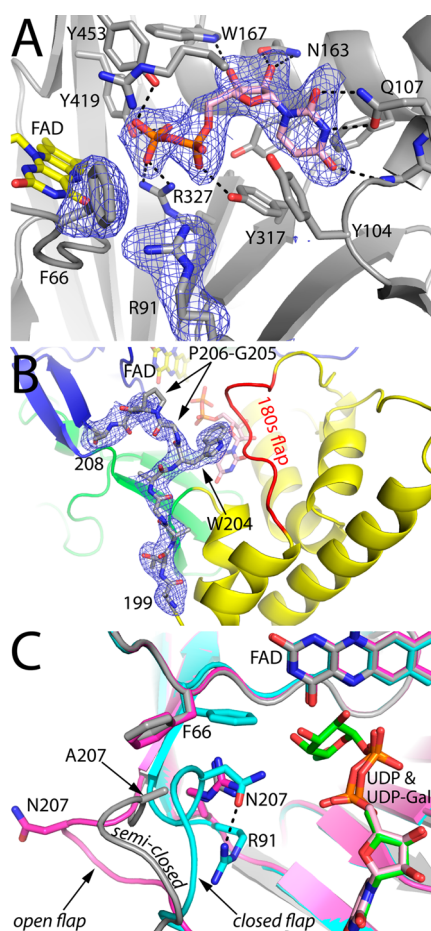
Figure 2. Structure of AfUGMF66A-UDP. (A) Electron density and interactions for UDP complexed to reduced AfUGMF66A. The mesh represents a simulated annealing $F_0 - F_c$ omit map (3σ). (B) Comparison of the active sites of AfUGMF66A-UDP (gray protein, pink UDP) and AfUGM-UDP-Gal$p$ (cyan protein, green UDP-Gal$p$). The two protein structures are essentially identical, except for the mutated residue.
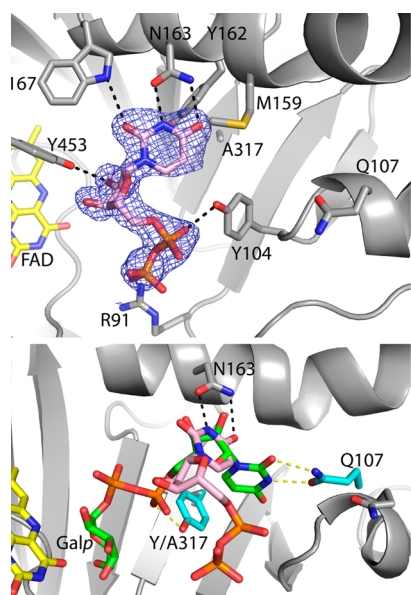

Figure 3. Structure of AfUGMN207A-UDP. (A) Electron density and interactions for UDP complexed to reduced AfUGMN207A. The mesh represents a simulated annealing $F_0 - F_c$ omit map (3σ). (B) Electron density for the semiclosed 200s flap of AfUGMN207A. The mesh represents a simulated annealing $F_0 - F_c$ omit map (2.5σ). (C) Comparison of the 200s flaps of flaps of ligand-free AfUGM (magenta), AfUGMN207A-UDP (gray), and AfUGM-UDP-Gal$p$ (cyan). UDP and UDP-Gal$p$ are colored pink and green, respectively. The dashed line indicates the Asn207-Arg91 hydrogen bond of AfUGM-UDP-Gal$p$.

As in AfUGMF66A-UDP, the conformation of UDP bound to AfUGMN207A is essentially identical to that bound to wild-type AfUGM (Figure 3A). Also, all the protein−ligand interactions in the wild-type enzyme complex are also observed in AfUGMN207A-UDP. Thus, the AfUGMN207A-UDP structure appears to mimic the Michaelis complex, at least in terms of the UDP portion of the substrate.

Although the UDP adopts the active conformation, the protein conformation of AfUGMN207A-UDP is a hybrid of the open and closed states of AfUGM. Similarly, the 180s flap adopts the closed conformation that is characteristic of the E-S complex; however, the 200s flap (residues 201−209) adopts a intermediate conformation (Figure 3B and C). The RMSD between AfUGMN207A-UDP and the wild-type enzyme UDP complex is just 0.1 Å for the 180s flap but 1.9 Å for the 200s flap. The deviation of the 200s flap from the closed conformation is most evident near residues Pro206-Ala207 (Figure 3C). This pair of residues is poised approximately 5 Å from the closed conformation and 10 Å from the open conformation. Thus, the 200s flap appears to have moved about two-thirds of the way along the pathway from open to closed.

A striking feature of AfUGMN207A-UDP is that Arg91 and Phe66 remain in their open conformations. These residues are close together in the left-hand side of the active site (as pictured in Figure 1B), and electron density for these side chains is very well-defined (Figure 3A). Previous structural studies have shown that in the wild-type enzyme, Arg91 moves by 5 Å to form a hydrogen bond with Asn207, while Phe66 rotates by 180° to contact the Gal$p$ moiety of the substrate (Figure 1B). Apparently, the binding of UDP has not provoked these

movements in the AfUGMN207A enzyme. These results suggest that the final 5 Å shift of the 200s flap from the semiclosed to closed conformation is required to induce movement of Arg91 and Phe66.

Crystal Structure of AfUGMY317A-UDP. In the structure of reduced AfUGMY317A, electron density for UDP is observed for all four protomers of the tetramer (Figure 4A). Occupancy refinement in PHENIX indicated occupancies of 0.79−0.83 (Table 4).

Mutation of Tyr317 to Ala profoundly alters substrate recognition (Figure 4). The uracil bound to AfUGMY317A occupies the ribose site of the wild-type enzyme, forming hydrogen bonds with Asn163. In this unexpected binding pose, the uracil is shifted by 5−6 Å relative to the wild-type enzyme-UDP/UDP-Gal$p$ complexes (Figure 4B). The ribose and pyrophosphate of UDP bound to AfUGMY317A occupy the space reserved for the 180s and 200s flaps of the wild-type enzyme complex. Thus, the bound UDP prevents flap closure. Indeed, not only are the flaps open, but the entire protein conformation of AfUGMY317A-UDP is virtually identical to

Figure 4. Structure of AfUGMY317A-UDP. (A) Electron density and interactions for UDP complexed to reduced AfUGMY317A. The mesh represents a simulated annealing $F_0 - F_c$ omit map (3σ). (B) Comparison of the conformations of UDP (pink) bound to AfUGMY317A and UDP-Gal*p* (green) bound to wild-type AfUGM. Side chains of AfUGMY317A are colored gray. Side chains of wild-type AfUGM are colored cyan. Black and yellow dashes represent hydrogen bonds in AfUGMY317A-UDP and AfUGM-UDP-Gal*p*, respectively.
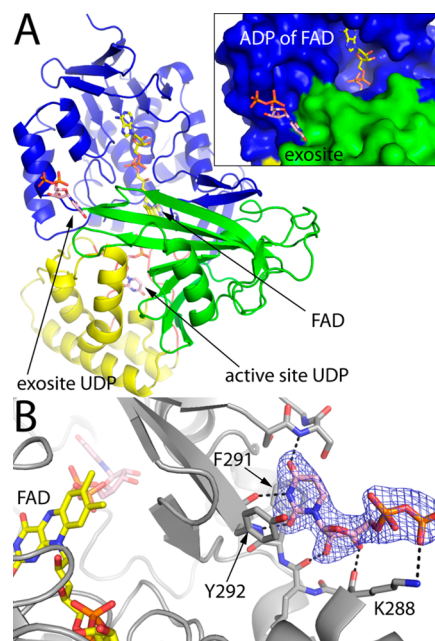

Figure 5. UDP exosite of AfUGMF66A. (A) Ribbon drawing of AfUGMF66A-UDP showing the location of the exosite. As in Figure 1, domains 1, 2, and 3 are colored blue, yellow, and green, respectively, and the active site flaps are red. The inset shows a surface representation of the exosite. (B) Electron density and interactions for UDP bound in the exosite. The mesh represents a simulated annealing $F_0 - F_c$ omit map (3σ).

that of the ligand-free AfUGM (RMSDs of 0.3 Å for the tetramer and less than 0.2 Å for the flaps). If UDP-Gal*p* binds to AfUGMY317A in this manner, the Gal*p* moiety would be approximately 10 Å from its normal position in the wild-type enzyme. Thus, the AfUGMY317A-UDP structure suggests that the mutation of Tyr317 to Ala promotes a catalytically nonproductive conformation of the substrate.

UDP Exosite. Electron density maps also suggested the presence of UDP bound in a pocket outside of the active site (Figure 5). The strength of the density varies among the protomers of a given tetramer and from protein to protein. In some cases, for example, strong density is evident only for the uridine portion of UDP. Protomer A of AfUGMF66A provides the best example of UDP bound in the exosite (Figure 5).

The exosite is located at a junction between domains 1 and 3 (Figure 5A). The uracil in the exosite UDP is 18 Å from the flavin N5 atom. The bound UDP interacts mainly with a loop that connects domains 1 and 3 (residues 288−292). The uracil is wedged between the side chains of Phe291 and Tyr292 and forms three hydrogen bonds to the protein backbone. The hydroxyls of the UDP ribose hydrogen bond to backbone carbonyls, while the pyrophosphate forms an ion pair with Lys288. The significance of the exosite is unclear.

■ DISCUSSION

Previous structural work showed that the active site conformations of ligand-free and substrate-bound AfUGM are very different, with the former being highly open and the latter tightly closed.[18] The structure of TcUGM-UDP shows the same closed active site.[34] Although the structure of ligand-free TcUGM has not been determined, sequence conservation and molecular dynamics simulations suggest that the conformational changes described for AfUGM also occur in TcUGM.[35]

For discussion purposes, the transition of eUGMs from open to closed can be deconstructed into five conformation changes: (1) closure of the 180s flap, (2) movement of Tyr104 away from and Gln107 toward the incoming uracil ring, (3) closure of the 200s flap, (4) movement of Arg91 to form a hydrogen bond to Asn207, and (5) rotation of Phe66 so that it contacts Gal*p*. The results reported here provide insight into the essentiality of these conformational changes for realizing maximal catalytic activity, the temporal order of conformational changes, and how the various aspects of active site closure are coupled.

Phe66 (Phe65 in TcUGM) has been called the "Gal*p* backstop" because it packs against the Gal*p* moiety of the substrate, and we previously suggested that the backstop is important for positioning Gal*p* for nucleophilic attack by the flavin N5.[9] Here, we probed the importance of this interaction with the AfUGMF66A mutation.

The AfUGMF66A-UDP structure is essentially identical to that of AfUGM complexed with UDP or UDP-Gal*p*. This result shows that rotation of Phe66 is not required for binding the UDP portion of the substrate in the catalytically correct conformation. However, since the activity of AfUGMF66A is compromised, the packing of Phe66 against the Gal*p* moiety apparently is necessary for full catalytic efficiency. This idea is consistent with the absence of strong electron density for Gal*p* in the AfUGMF66A-UDP-Gal*p* structure (Supporting Information Figure S2). We noted previously that bacterial UGMs have a conserved His in place of AfUGM Phe66 and suggested that the His may also function as the Gal*p* backstop. Using the UGM from *M. tuberculosis* we tested this hypothesis by determining the activity of MtUGMH68A (Table 1). This mutant UGM displays a similar decrease in activity as
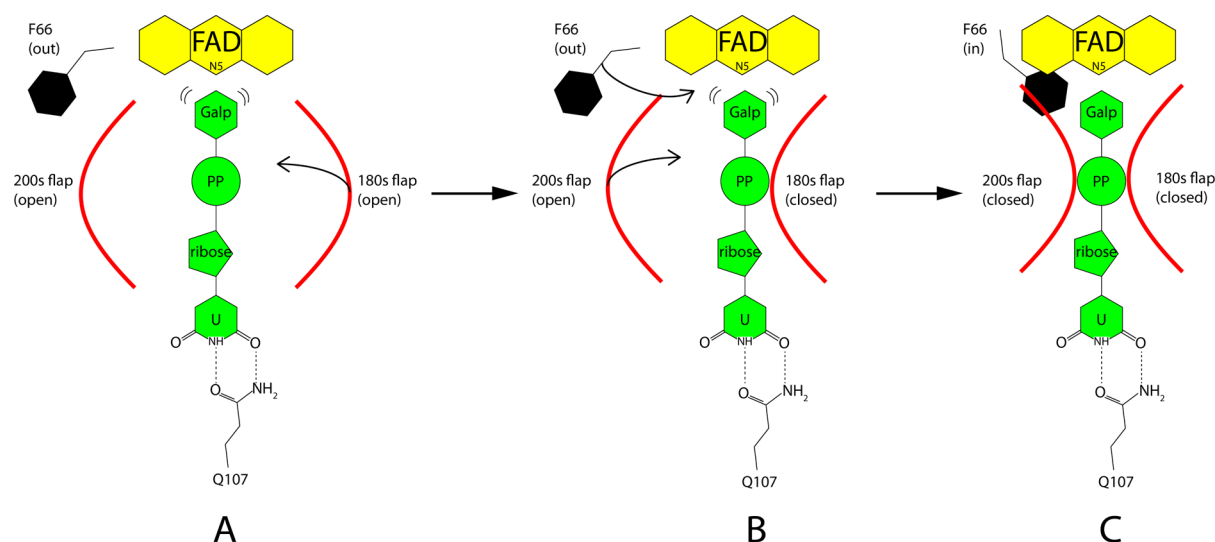
Figure 6. Cartoon depicting the possible sequence of active site conformations that are populated during substrate binding. (A) UMP docks into the active site and forms hydrogen bonds with Gln107. (B) The 180s flap closes. (C) The 200s flap closes as Phe66 rotates to the "in" conformation.

AfUGMF66A, supporting the role of the conserved His in bacterial UGM as the Gal*p* backstop.

We investigated the role of Asn207 with the AfUGMN207A and TcUGMN201A variants. This residue is known as the "mobile Asn" because it moves by 10 Å during the closing transition.[9] In the closed state, Asn207 (Asn201 in TcUGM) form a hydrogen bond with Arg91 (Arg87 in TcUGM), an interaction that has been suggested to stabilize the closed active site conformation.[9,18] Absence of the Asn207-Arg91 interaction in AfUGMN207A appears to prevent the 200s flap from forming the true closed conformation when UDP is bound, instead adopting a semiclosed conformation (Figure 3C). These results suggest that the Asn207-Arg91 hydrogen bond is essential for full closure of the 200s flap, and complete flap closure is necessary for full catalytic efficiency. This analysis is consistent with molecular dynamics simulations that show the equivalent residue in TcUGM (Asn201) is involved in opening/closure of the 200 loop via interactions with Gal*p*.[35]

Another interesting characteristic of the AfUGMN207A-UDP structure is that Phe66 remains in the open conformation; it does not rotate into the active site as in the structures of the wild-type enzyme complexed with UDP or UDP-Gal*p*. This result suggests that rotation of Phe66 is coupled to closure of the 200s flap. Steric repulsion is the likely coupling mechanism. Upon substrate (or UDP) binding, Pro206 invades the space occupied by Phe66, forcing rotation of Phe66 to avoid steric clash. In the semiclosed conformation in AfUGMN207A-UDP, Pro206 has not moved far enough to displace Phe66 (Figure 3C).

The AfUGMY317A-UDP structure along with the kinetics of AfUGMY317A and TcUGMY317F suggest an essential role for Tyr317 in substrate recognition. UDP binds to Y317A in a catalytically nonproductive conformation in which the implied Gal*p* moiety would be directed away from the isoalloxazine and toward the active site entrance. A salient feature of the structure is the 5−6 Å misplacement of the uracil (Figure 4B). It thus appears that Tyr317, by hydrogen bonding to the pyrophosphate, is essential for directing the UMP into its correct binding pocket. Site directed mutagenesis of Tyr residues in *K. pneumonia* UGM showed that Tyr resides that are predicted to interact with the pyrophosphate moiety of UDP decrease the

k_{cat}/K_M value of only 10-fold, with the major effect originating from increase in the K_M value.[36] The overall contribution to catalysis of active site Tyr residues in eUGMs is much greater than in the bacterial counterparts. We propose that this might be due to the larger flexibility of the active site in the eUGMs.

Activation of eUGMs has been demonstrated to occur via the stereospecific transfer of the *pro*-R hydride equivalent of NADPH to reduce the flavin. We previously showed that the binding sites for NADPH and UDP-Gal*p* are distinct, although both the nicotinamide of NADPH and the Gal*p* of UDP-Gal*p* must be close to the isoalloxazine for activity.[22] Analysis of the reaction of the AfUGM mutants studied here with NADPH shows minimal changes in the k_{red} of K_D values. These results further show that the active site architecture of eUGM contains unique and separate binding interactions for UDP-Gal*p* and NADPH.

The structures provide a hypothesis for the order of conformational changes that accompany substrate binding. The fact that the active site is completely open in AfUGMY317A-UDP is consistent with the idea that docking of the UMP group and formation of the uracil-Gln107 hydrogen bonds occur early in active site closure. The observation in AfUGMN207A that the 180s flap is fully closed while the 200s flap is semiclosed supports the idea that the 180s flap achieves the closed conformation before the 200s flap has finished closing, although we acknowledge that mutational analysis of 180s flap is needed to further support this hypothesis. Finally, the fact that the open conformation of Phe66 would clash with the closed 200s loop suggests that rotation of Phe66 likely occurs in concert with closure of the 200s loop. Collectively, the structures suggest that closure of the active site begins with the docking of the UMP group (Figure 6A), followed by closure of the 180s flap (Figure 6A−B) and the concerted rotation of Phe66 and movement of the 200s flap (Figure 6B−C). These conformational changes likely occur in TcUGM, based on the strong sequence identity of the active sites of eUGMs and the high structural similarity of the AfUGM-UDP and TcUGM-UDP complexes. Since analogous TcUGM and AfUGM mutants display similar kinetic phenotypes, the results described here can be extended other members of the eUGM family.

Finally, the structures revealed a new, low affinity binding site for UDP located 18 Å from the flavin N5 atom. Density for UDP was observed in all the mutant enzyme structures, indicating that binding to this site is not an artifact of any particular mutation. The exosite of wild-type AfUGM is unoccupied at soaking concentration of 40 mM (see PDB 3UTG) and is weakly occupied at 200 mM UDP (data not shown). Thus, the exosite has low affinity for UDP. The apparent low affinity suggests that the exosite is physiologically irrelevant. Also, the structures show that binding of UDP to the exosite does not inhibit binding of UDP to the active site. Thus, the exosite does not play a role in catalysis or regulation. On the other hand, the exosite is reminiscent of the sites revealed by fragment-based lead discovery. Very high ligand concentrations are used in fragment-based methods to discover low affinity[37] compounds that serve as starting points for designing high affinity inhibitors. Analogously, it is temping to consider the possibility of exploiting the exosite in the design of molecules that inhibit the activity of AfUGM.

■ ASSOCIATED CONTENT

Ⓢ Supporting Information

Two supplemental figures. This material is available free of charge via the Internet at http://pubs.acs.org.

Accession Codes

Atomic coordinates and structure factor amplitudes have been deposited in the Protein Data Bank as entries 4U8I (AfUGMF66A), 4U8J (AfUGMY104A), 4U8K (AfUGM-Q107A), 4U8L (AfUGMN207A), 4U8M (AfUGMY317A), 4U8N (AfUGMF66A-UDP), 4U8O (AfUGMN207A-UDP), 4U8P (AfUGMY317A-UDP), and 4WX1 (AfUGMF66A-UDP-Gal*p*).

■ AUTHOR INFORMATION

Corresponding Authors

*E-mail: tannerjj@missouri.edu. Phone: (573) 884-1280. Fax: (573) 882-2754.
*E-mail: psobrado@vt.edu. Phone (540) 231-9485. Fax (540) 231-9070.

Author Contributions

Isabel Da Fonseca and Insaf A. Qureshi contributed equally to this work.

Notes

The authors declare no competing financial interest.

■ ACKNOWLEDGMENTS

■ ABBREVIATIONS

UGM, UDP-galactopyranose mutase; UDP-Gal*p*, UDP-galactopyranose; UDP-Gal*f*, UDP-galactofuranose; AfUGM, UDP-galactopyranose mutase from *Aspergillus fumigatus*; TcUGM, UDP-galactopyranose mutase from *Trypanosoma cruzi*; MtUGM, UDP-galactopyranose mutase from *Mycobacterium tuberculosis*; PDB, Protein Data Bank; RMSD, root-mean-square deviation

■ REFERENCES

(1) Richards, M. R., and Lowary, T. L. (2009) Chemistry and biology of galactofuranose-containing polysaccharides. *ChemBioChem* 10, 1920−1938.
(2) Latge, J. P. (2009) Galactofuranose containing molecules in Aspergillus fumigatus. *Med. Mycol.* 47 (Suppl.1), S104−109.
(3) Weston, A., Stern, R. J., Lee, R. E., Nassau, P. M., Monsey, D., Martin, S. L., Scherman, M. S., Besra, G. S., Duncan, K., and McNeil, M. R. (1997) Biosynthetic origin of mycobacterial cell wall galactofuranosyl residues. *Tuber. Lung Dis.* 78, 123−131.
(4) Pan, F., Jackson, M., Ma, Y., and McNeil, M. (2001) Cell wall core galactofuran synthesis is essential for growth of mycobacteria. *J. Bacteriol.* 183, 3991−3998.
(5) Kizjakina, K., Tanner, J. J., and Sobrado, P. (2013) Targeting UDP-galactopyranose mutases from eukaryotic human pathogens. *Curr. Pharm. Des.* 19, 2561−2573.
(6) Oppenheimer, M., Valenciano, A. L., and Sobrado, P. (2011) Biosynthesis of galactofuranose in kinetoplastids: novel therapeutic targets for treating leishmaniasis and chagas' disease. *Enzyme Res.* 2011, 415976.
(7) Tefsen, B., Ram, A. F., van Die, I., and Routier, F. H. (2012) Galactofuranose in eukaryotes: aspects of biosynthesis and functional impact. *Glycobiology* 22, 456−469.
(8) Nassau, P. M., Martin, S. L., Brown, R. E., Weston, A., Monsey, D., McNeil, M. R., and Duncan, K. (1996) Galactofuranose biosynthesis in Escherichia coli K-12: identification and cloning of UDP-galactopyranose mutase. *J. Bacteriol.* 178, 1047−1052.
(9) Tanner, J. J., Boechi, L., Andrew McCammon, J., and Sobrado, P. (2014) Structure, mechanism, and dynamics of UDP-galactopyranose mutase. *Arch. Biochem. Biophys.* 544, 128−141.
(10) Zhang, Q., and Liu, H-w. (2000) Studies of UDP-Galactopyranose mutase from Escherichia coli: An Unusual Role of Reduced FAD in Its Catalysis. *J. Am. Chem. Soc.* 122, 9065−9070.
(11) Soltero-Higgin, M., Carlson, E. E., Gruber, T. D., and Kiessling, L. L. (2004) A unique catalytic mechanism for UDP-galactopyranose mutase. *Nat. Struct. Mol. Biol.* 11, 539−543.
(12) Oppenheimer, M., Poulin, M. B., Lowary, T. L., Helm, R. F., and Sobrado, P. (2010) Characterization of recombinant UDP-galactopyranose mutase from Aspergillus fumigatus. *Arch. Biochem. Biophys.* 502, 31−38.
(13) Soltero-Higgin, M., Carlson, E. E., Phillips, J. H., and Kiessling, L. L. (2004) Identification of inhibitors for UDP-galactopyranose mutase. *J. Am. Chem. Soc.* 126, 10532−10533.

(14) Gruber, T. D., Westler, W. M., Kiessling, L. L., and Forest, K. T. (2009) X-ray crystallography reveals a reduced substrate complex of UDP-galactopyranose mutase poised for covalent catalysis by flavin. *Biochemistry 48*, 9171−9173.

(15) Oppenheimer, M., Valenciano, A. L., Kizjakina, K., Qi, J., and Sobrado, P. (2012) Chemical mechanism of UDP-galactopyranose mutase from Trypanosoma cruzi: a potential drug target against Chagas' disease. *PLoS One 7*, e32918.

(16) Dykhuizen, E. C., May, J. F., Tongpenyai, A., and Kiessling, L. L. (2008) Inhibitors of UDP-galactopyranose mutase thwart mycobacterial growth. *J. Am. Chem. Soc. 130*, 6706−6707.

(17) Damveld, R. A., Franken, A., Arentshorst, M., Punt, P. J., Klis, F. M., van den Hondel, C. A., and Ram, A. F. (2008) A novel screening method for cell wall mutants in Aspergillus niger identifies UDP-galactopyranose mutase as an important protein in fungal cell wall biosynthesis. *Genetics 178*, 873−881.

(18) Dhatwalia, R., Singh, H., Oppenheimer, M., Karr, D. B., Nix, J. C., Sobrado, P., and Tanner, J. J. (2012) Crystal structures and small-angle x-ray scattering analysis of UDP-galactopyranose mutase from the pathogenic fungus Aspergillus fumigatus. *J. Biol. Chem. 287*, 9041−9051.

(19) Sun, H. G., Ruszczycky, M. W., Chang, W. C., Thibodeaux, C. J., and Liu, H. W. (2012) Nucleophilic participation of reduced flavin coenzyme in mechanism of UDP-galactopyranose mutase. *J. Biol. Chem. 287*, 4602−4608.

(20) Rose, N. L., Zheng, R. B., Pearcey, J., Zhou, R., Completo, G. C., and Lowary, T. L. (2008) Development of a coupled spectrophotometric assay for GlfT2, a bifunctional mycobacterial galactofuranosyltransferase. *Carbohydr. Res. 343*, 2130−2139.

(21) Blommel, P. G., Becker, K. J., Duvnjak, P., and Fox, B. G. (2007) Enhanced bacterial protein expression during auto-induction obtained by alteration of lac repressor dosage and medium composition. *Biotechnol. Prog. 23*, 585−598.

(22) Dhatwalia, R., Singh, H., Solano, L. M., Oppenheimer, M., Robinson, R. M., Ellerbrock, J. F., Sobrado, P., and Tanner, J. J. (2012) Identification of the NAD(P)H binding site of eukaryotic UDP-galactopyranose mutase. *J. Am. Chem. Soc. 134*, 18132−18138.

(23) Oppenheimer, M., Poulin, M. B., Lowary, T. L., Helm, R. F., and Sobrado, P. (2010) Characterization of recombinant UDP-galactopyranose mutase from Aspergillus fumigatus. *Arch. Biochem. Biophys. 502*, 31−38.

(24) Kabsch, W. (2010) Xds. *Acta Crystallogr. D66*, 125−132.

(25) Evans, P. (2006) Scaling and assessment of data quality. *Acta Crystallogr. D62*, 72−82.

(26) Evans, P. R. (2011) An introduction to data reduction: space-group determination, scaling and intensity statistics. *Acta Crystallogr. D67*, 282−292.

(27) Adams, P. D., Afonine, P. V., Bunkoczi, G., Chen, V. B., Davis, I. W., Echols, N., Headd, J. J., Hung, L. W., Kapral, G. J., Grosse-Kunstleve, R. W., McCoy, A. J., Moriarty, N. W., Oeffner, R., Read, R. J., Richardson, D. C., Richardson, J. S., Terwilliger, T. C., and Zwart, P. H. (2010) PHENIX: a comprehensive Python-based system for macromolecular structure solution. *Acta Crystallogr. D66*, 213−221.

(28) Emsley, P., and Cowtan, K. (2004) Coot: model-building tools for molecular graphics. *Acta Crystallogr. D60*, 2126−2132.

(29) Chen, V. B., Arendall, W. B., 3rd, Headd, J. J., Keedy, D. A., Immormino, R. M., Kapral, G. J., Murray, L. W., Richardson, J. S., and Richardson, D. C. (2010) MolProbity: all-atom structure validation for macromolecular crystallography. *Acta Crystallogr. D66*, 12−21.

(30) Lovell, S. C., Davis, I. W., Arendall, W. B., 3rd, de Bakker, P. I., Word, J. M., Prisant, M. G., Richardson, J. S., and Richardson, D. C. (2003) Structure validation by Calpha geometry: phi,psi and Cbeta deviation. *Proteins 50*, 437−450.

(31) Da Fonseca, I., Kizjakina, K., and Sobrado, P. (2013) UDP-galactopyranose mutases from Leishmania species that cause visceral and cutaneous leishmaniasis. *Arch. Biochem. Biophys. 538*, 103−110.

(32) Zhang, Q., and Liu, H. W. (2000) Studies of UDP-galactrpyranose mutase from Escerichia coli: an unusual role of reduced FAD in its catalysis. *J. Am. Chem. Soc. 122*, 9065−9070.

(33) van Straaten, K. E., Routier, F. H., and Sanders, D. A. (2012) Structural insight into the unique substrate binding mechanism and flavin redox state of UDP-galactopyranose mutase from Aspergillus fumigatus. *J. Biol. Chem. 287*, 10780−10790.

(34) Dhatwalia, R., Singh, H., Oppenheimer, M., Sobrado, P., and Tanner, J. J. (2012) Crystal structures of Trypanosoma cruzi UDP-galactopyranose mutase implicate flexibility of the histidine loop in enzyme activation. *Biochemistry 51*, 4968−4979.

(35) Boechi, L., de Oliveira, C. A., Da Fonseca, I., Kizjakina, K., Sobrado, P., Tanner, J. J., and McCammon, J. A. (2013) Substrate-dependent dynamics of UDP-galactopyranose mutase: Implications for drug design. *Protein Sci. 11*, 1490−501.

(36) Chad, J. M., Sarathy, K. P., Gruber, T. D., Addala, E., Kiessling, L. L., and Sanders, D. A. (2007) Site-directed mutagenesis of UDP-galactopyranose mutase reveals a critical role for the active-site, conserved arginine residues. *Biochemistry 46*, 6723−6732.

(37) Murray, C. W., and Rees, D. C. (2009) The rise of fragment-based drug discovery. *Nat. Chem. 1*, 187−192.